https://doi.org/10.15407/ujpe71.9.717

N.M. BLASHKO,[1] O.V. MARCHUK,[1] V.M. HREB,[2] R.L. BUKLIV,[2] M.YA. RUDYSH[3]

[1] Lesya Ukrainka Volyn National University
(13, Voli Ave., Lutsk 43025, Ukraine; e-mail: blashko.nazarii@vnu.edu.ua)
[2] Lviv Polytechnic National University
(12, Stepana Bandery Str., Lviv 79000, Ukraine; e-mail: roksoliana.l.bukliv@lpnu.edu.ua)
[3] Ivan Franko National University of Lviv
(8, Kyryla and Mefodiia Str., Lviv 7900, Ukraine; e-mail: myron.rudysh@lnu.edu.ua)

CRYSTAL CHEMISTRY, OPTICAL PROPERTIES AND ELECTRONIC STRUCTURE OF $R_3Fe_{0.1}Ga_{1.6}S_7$ (R – La, Ce, Pr, Nd, Tb) SULFIDES

X-ray powder diffraction data were used to determine the crystal chemical parameters of $R_3Fe_{0.1}Ga_{1.6}S_7$ (R – La, Ce, Pr, Nd, Tb) sulfides, which crystallize in the La_3CuSiS_7 structural type (space group (SG) $P6_3$). The crystal structure of these compounds is formed by an interconnected three-dimensional framework of various coordination polyhedral types, including seven-coordinated [R S_7] polyhedra, mixed-occupancy [M (Fe, Ga) S_6] octahedra, and [Ga S_4] tetrahedra. The qualitative and quantitative elemental composition of the synthesized sulfides was confirmed by energy-dispersive X-ray spectroscopy combined with scanning electron microscopy (EDX/SEM). Dynamic light scattering was used to characterize the particle size distribution and degree of homogeneity in colloidal systems (dispersion in isopropyl alcohol) to determine the polydispersity indices. The optical parameters of the sulfides were determined using the Tauc plot method, revealing band gaps from 1.95 to 2.50 eV for direct interband transitions and from 1.21 to 2.70 eV for indirect ones, demonstrating composition-dependent variability of the electronic structure. For the sulfides containing La and Ce, quantum-chemical modeling was performed within the framework of density functional theory (DFT; ab initio approach) to calculate the band structure.

K e y w o r d s: rare-earth elements (REE), energy-dispersive X-ray spectroscopy, X-ray powder diffraction, Tauc plot method, density functional theory.

1. Introduction

Complex chalcogenide compounds with the generalized formulas $R_3A_{0.45}Ga_{1.52}X_7$ and $R_3B_{0.1}Ga_{1.6}X_7$ (where R represents rare-earth ions; A represents monovalent metals Cu or Ag; B represents 3*d* transition metals Mn, Fe, Co, or Ni; X represents chalcogens S or Se) are the objects of targeted and systematic studies [1–4]. The relevance of studying such objects is driven by their multifunctional physicochemical profile, which includes a wide range of optical, thermal, electrical, and magnetic properties determined by their complex crystal chemistry and electronic structure.

Chalcogenide materials (sulfides, selenides, tellurides) currently hold an important place among functional compounds for high-tech applications. Due to their wide transparency window and ability to exhibit significant nonlinear optical susceptibility (particularly of the second order in noncentrosymmetric structures), they are important for IR spectroscopy, laser technology, and the development of mid-IR waveguides [5, 6]. In addition to their optical properties, these compounds are actively investigated as efficient thermoelectrics and as a basis for non-volatile phase-change memory [7–9].

Gallium-containing chalcogenides [10–14] with a noncentrosymmetric crystal structure of the $P6_3$ type attract particular attention, since the absence of

C i t a t i o n: Blashko N.M., Marchuk O.V., Hreb V.M., Bukliv R.L., Rudysh M.Ya. Crystal chemistry, optical properties and electronic structure of $R_3Fe_{0.1}Ga_{1.6}S_7$ (R – La, Ce, Pr, Nd, Tb) sulfides. *Ukr. J. Phys.* **71**, No. 9, 717 (2026). https://doi.org/10.15407/ujpe71.9.717.

an inversion center is a necessary condition for the emergence of quadratic nonlinear optical susceptibility. This, in particular, enables second-harmonic generation, which is of key importance in laser frequency doubling and parametric generation processes [15]. Materials with such structural features are considered a promising platform for the development of a new generation of photonic and optoelectronic components due to their high laser damage threshold and significant values of nonlinear optical coefficients [16].

Of particular interest are sulfides of the $R_3Fe_{0.1}Ga_{1.6}S_7$ type, in which the combination of rare-earth elements with partially filled *d*- and *f*-electron states and a statistical mixture of cations in the crystal lattice results in high sensitivity of the electronic structure to compositional changes. This provides opportunities for the targeted control of their optical and electronic characteristics, which is crucial for creating functional materials for optoelectronics.

2. Experimental

The synthesis of sulfides was carried out by direct ampoule synthesis using simple substances of semiconductor purity in quartz containers evacuated down to 10^{-2} Pa. The weighed portions of the starting batch, weighing 1.0 g each, were subjected to heat treatment according to the following regime: heating to a temperature of 400 °C at a rate of 30 °C/h (holding for 4 h); heating to a temperature of 1100 °C at a rate of 12 °C/h (holding for 4 h); slow cooling (6 °C/h) to a temperature of 500 °C. At this temperature, homogenization annealing was performed for one month to achieve phase homogeneity of the synthesized samples. To preserve the achieved structural state, the annealed samples were quenched in water at room temperature (∼22 °C).

Structural investigations were performed using X-ray powder diffraction method on a DRON 4-13 diffractometer using CuK_α radiation. Crystal structure refinement was carried out by the Rietveld method using the WinCSD software package [17], and the visualization of the structural model was performed using the VESTA software package [18].

The hydrodynamic sizes of $R_3Fe_{0.1}Ga_{1.6}S_7$ particles dispersed in isopropyl alcohol were determined by dynamic light scattering (DLS), based on measurements of random changes in the intensity of light scattered by the suspension, using a DynaPro NanoStar (Wyatt Technology, USA) with noninvasive backscattering technology at a temperature of 298 K. The concentration of the samples was 5 mg/cm^3. Before the measurements, the suspension was subjected to ultrasonic dispersion for 10 seconds. For this purpose, a high-frequency ultrasonic homogenizer UZDN-1A (Sumy, Ukraine) with a frequency of 22 kHz and a power of 40 W was used.

For the analysis of the suspensions, three series of measurements were performed at five-minute intervals. Each series included ten consecutive measurement cycles, the results of which were automatically averaged and processed using the built-in software of the measuring instrument. This approach allowed the effect of random fluctuations to be minimized and representative data on the stability of the system to be obtained. The average hydrodynamic diameter indicates a relatively narrow distribution and homogeneity of the particles in the system.

Particle polydispersity (polydispersity index, PDI) was calculated using the formula:

$$\mathrm{PDI} = (SD)^2/(D_h)^2, \tag{1}$$

where SD is the standard deviation of particle sizes, nm; D_h is the mean hydrodynamic diameter determined by DLS, nm.

The diffuse reflectance spectra of the synthesized sulfides were recorded using a Shimadzu 3600i Plus spectrophotometer equipped with an MPC-603A multipurpose sample compartment and an integrating sphere in the wavelength range of 200–1500 nm at a temperature of 293 K. Barium sulfate was used as a white reference standard for the spectral measurements. To analyze the obtained diffuse reflectance spectra, the Kubelka–Munk mathematical model [19] was applied, which relates the absorption K and scattering S coefficients to the reflectance function of the material, $F(R)$:

$$F(R) = K/S = (1-R)^2/2R \tag{2}$$

and the Tauc function [20], which was used to estimate the band gap energies of the investigated polycrystalline sulfides. The Tauc function is expressed by the equation:

$$(\alpha \cdot hv)^n = A \cdot (hv - E_g), \tag{3}$$

where α is the absorption coefficient proportional to the Kubelka–Munk function $F(R)$, R is the diffuse reflectance, h is Planck's constant, v is the photon frequency, E_g is the band gap energy, and A is a material-dependent constant. The exponent n depends on the nature of the electronic transition and equals $n = 2$ or $n = 1/2$ for direct and indirect allowed transitions, respectively.

The electronic structure of $R_3Fe_{0.1}Ga_{1.6}S_7$ (R – La, Ce) sulfides was investigated using density functional theory within the Kohn–Sham formalism [21]. The practical implementation of this theory was carried out using the CASTEP software package [22, 23]. The crystallographic data for $R_3Fe_{0.1}Ga_{1.6}S_7$ (R – La, Ce) obtained in this work by the XRD method were used as initial parameters for the calculations of material properties. Crystal structure modeling with a statistical distribution of certain chemical elements was carried out using the mixed atom method within the virtual crystal approximation [24]. No geometry optimization was performed prior to the calculations. The total energy of the system was obtained from a self-consistent solution of the Kohn–Sham equations. The wave functions of the valence electrons were expanded in a basis of Bloch-type plane waves. The electronic configuration of the valence electrons was as follows: La – $5d^1\ 6s^2$; Ce – $4f^1\ 5s^2\ 5p^6\ 6s^2$; Ga – $3d^{10}\ 4s^2\ 4p^1$; Fe – $3s^2\ 3p^6\ 3d^6\ 4s^2$; S – $3s^2\ 3p^4$. The plane-wave cutoff energy was set to $E_{\text{cut}} = 900$ eV. The norm-conserving pseudopotential method [25] was used to describe the core electrons. The exchange-correlation interaction was treated within the generalized gradient approximation (GGA) parameterized by Perdew–Burke–Ernzerhof (PBE). Brillouin zone integration was performed over a $4 \times 4 \times 6$ k-point grid generated according to the Monkhorst–Pack scheme [26].

3. Results and Discussion

The $R_3Fe_{0.1}Ga_{1.6}S_7$ sulfides were synthesized by targeted modification of $R_3Ga_{1.67}S_7$ compounds [27–29], whose crystal structure belongs to the La_3CuSiS_7 structural type (SG $P6_3$) [30]. The structural modification involved the partial substitution of Ga atoms at the 2a site by divalent iron atoms. As a result, a statistical mixture of M (Fe + Ga) atoms forms at the 2a site, which ensures charge compensation and helps reduce local structural stresses associated with deviations from the ideal stoichiometry of the initial compounds. The crystallographic features of individual members of this series are described in detail in our previous work [3].

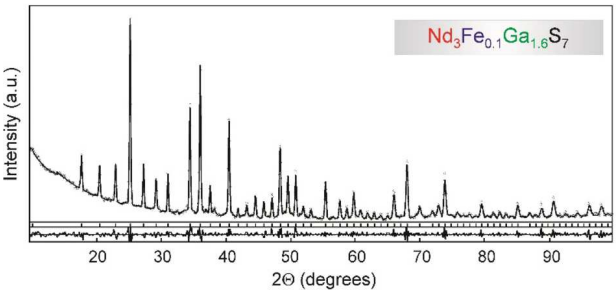

Fig. 1. Observed, calculated, and difference XRD patterns of $Nd_3Fe_{0.1}Ga_{1.6}S_7$

Table 1. **Atomic coordinates and isotropic displacement parameters in the structure of $Nd_3Fe_{0.1}Ga_{1.6}S_7$**

$a = 9.9071(5)$ Å, $c = 6.0690(6)$ Å, $V = 515.87(9)$ Å^3, $R_I = 0.0747$, $R_P = 0.2148$					
Atoms	site	x/a	y/b	z/c	B_{iso} Å^2
Nd	6 c	0.3777(2)	0.1488(4)	0.234(2)	0.26(6)
M	2 a	0	0	–0.014(8)	0.8(5)
Ga	2 b	1/3	2/3	0.159(2)	0.3(4)
S1	6 c	0.0938(10)	0.511(3)	0.009(4)	0.6(5)
S2	6 c	0.1366(11)	0.242(2)	0.290(3)	0.4(4)
S3	2 b	1/3	2/3	0.531(7)	0.3(8)

The observed, calculated, and difference XRD patterns for the iron-containing sulfide $Nd_3Ga_{1.67}S_7$ based on $Nd_3Fe_{0.1}Ga_{1.6}S_7$ are presented in Fig. 1.

The refined atomic coordinates and isotropic displacement parameters for the sulfide structure are presented in Table 1.

The unit cell and coordination polyhedra characteristic of the structure of $R_3Fe_{0.1}Ga_{1.6}S_7$ (R – La, Ce, Pr, Nd, Tb; M – 0.1 Fe + 0.6 Ga) sulfides are shown in Fig. 2.

An ordered arrangement of rare-earth element, gallium, iron, and sulfur atoms is realized in these structures, forming a three-dimensional framework. The R atoms are localized at the 6c crystallographic position and coordinate seven sulfur atoms to form distorted trigonal prisms [$R^{(6c)}\ 6S^{(6c)}1S^{(2b)}$]. These polyhedra serve as the primary structure-forming elements of

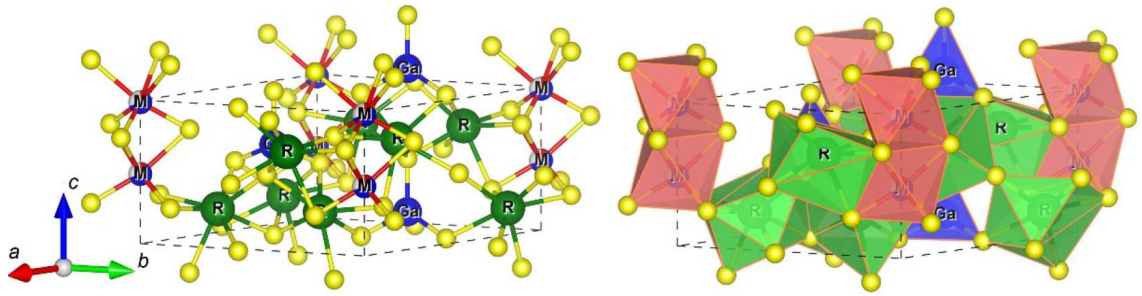

a *b*

Fig. 2. Unit cell (*a*) and coordination polyhedra (*b*) [$R^{(6c)}$ $6S^{(6c)}1S^{(2b)}$], [$M^{(2a)}$ $6S^{(6c)}$] and [$Ga^{(2b)}$ $3S^{(6c)}1S^{(2b)}$] in the structure of $R_3Fe_{0.1}Ga_{1.6}S_7$ (R – La, Ce, Pr, Nd, Tb; M – 0.1 Fe + 0.6 Ga)

the cationic sublattice. The 2*a* site is statistically occupied by M (M – 0.1 Fe + 0.6 Ga), with the Fe content in this statistical mixture being negligible. The M atoms are surrounded by six sulfur atoms, forming octahedral polyhedra [$M^{(2a)}$ $6S^{(6c)}$]. The octahedra are characterized by a certain degree of distortion, which arises from the statistical occupancy of the 2*a* position by atoms of different chemical nature and ionic radii.

The Ga atoms localized at the 2*b* site have a tetrahedral coordination environment of sulfur atoms and form [$Ga^{(2b)}$ $3S^{(6c)}1S^{(2b)}$] tetrahedra. Tetrahedral coordination is characteristic of gallium in chalcogenide structures and indicates a predominantly covalent nature of the Ga–S bonds. The tetrahedra are spatially isolated from each other and are connected to the [$R^{(6c)}$ $6S^{(6c)}1S^{(2b)}$] and [$M^{(2a)}$ $6S^{(6c)}$] polyhedra through shared sulfur-atom vertices.

As shown in Fig. 3, *a*, the $La_3Fe_{0.1}Ga_{1.6}S_7$ compound exhibits slight polydispersity, with a particle radius ranging from ∼577 to ∼733 nm and a standard deviation of ±455 nm. This could be due to the partial sedimentation of larger particles. The value of the polydispersity index is PDI ≈ 0.156.

For the $Ce_3Fe_{0.1}Ga_{1.6}S_7$ structure, the particle dispersion is stable and characterized by a unimodal distribution with a particle radius of ∼138 nm, a standard deviation of ±109 nm and a polydispersity index PDI ≈ 0.154 (Fig. 3, *b*).

The particle dispersion of the synthesized $Pr_3Fe_{0.1}Ga_{1.6}S_7$ sulfide (Fig. 3, *c*) is also stable and characterized by a unimodal distribution with a particle radius ranging from ∼109 to ∼139 nm, a standard deviation of ±97 nm, and a polydispersity index PDI ≈ 0.154.

The particle dispersion for the $Nd_3Fe_{0.1}Ga_{1.6}S_7$ structure (Fig. 3, *d*) is stable and characterized by a unimodal distribution, with a particle radius of ∼139 nm, a standard deviation of ±109 nm, and a polydispersity index PDI ≈ 0.154.

An analysis of the curves in Fig. 3, *e* shows that for the $Tb_3Fe_{0.1}Ga_{1.6}S_7$ structure, as with the previous structures, the particle dispersion is stable and characterized by a unimodal distribution, with a particle radius of ∼359 nm, a standard deviation in particle size of ±283 nm, and a polydispersity index PDI ≈ 0.154.

The higher polydispersity of the synthesized $La_3Fe_{0.1}Ga_{1.6}S_7$ sulfide compared to $R_3Fe_{0.1}Ga_{1.6}S_7$ (R – Ce, Pr, Nd, Tb) sulfides can be explained by the specific electronic structure of the lanthanum atom, $[Xe]6s^25d^1$. The other synthesized rare-earth sulfides are characterized by the gradual filling of the *f*-subshell. This causes a decrease in the orbital radius of the ions due to the *f*-contraction effect and, consequently, the formation of a more unimodal particle size distribution.

The measured diffuse reflectance spectra for the investigated $R_3Fe_{0.1}Ga_{1.6}S_7$ (R – La, Ce, Pr, Nd and Tb) chalcogenide powders are presented in Fig. 4. It is known that rare-earth metal ions absorb energy at characteristic wavelengths [31]. For the $La_3Fe_{0.1}Ga_{1.6}S_7$ sulfide, the spectra exhibit a clear band gap with no additional characteristic lines arising from transitions between the energy levels of lanthanum, since the *f*-levels that determine the functional properties are completely empty. The band gap energy in lanthanum compounds is determined by the separation between the *p*-states of the anion and the 5*d*-states of La [32].

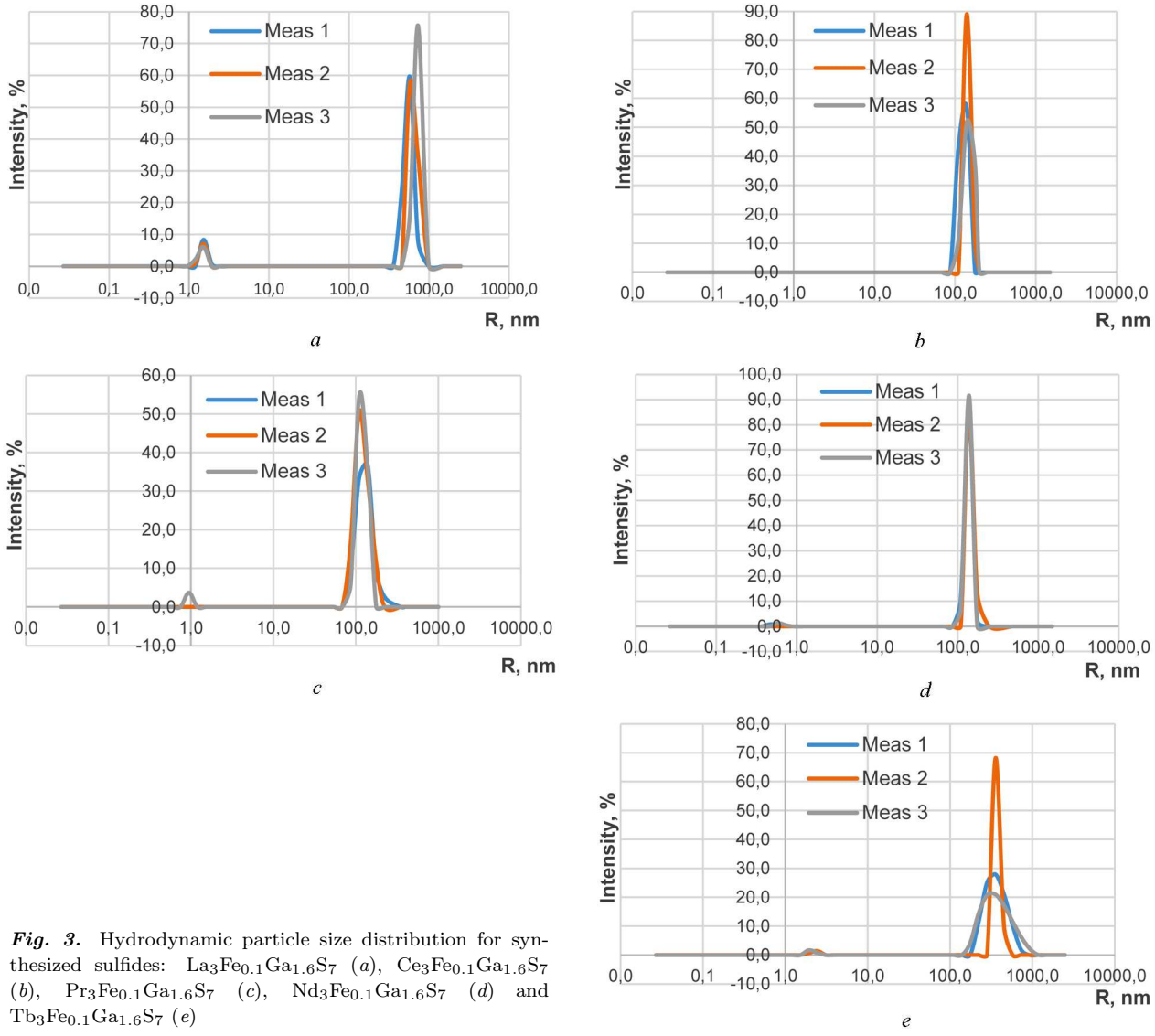

Fig. 3. Hydrodynamic particle size distribution for synthesized sulfides: $La_3Fe_{0.1}Ga_{1.6}S_7$ (*a*), $Ce_3Fe_{0.1}Ga_{1.6}S_7$ (*b*), $Pr_3Fe_{0.1}Ga_{1.6}S_7$ (*c*), $Nd_3Fe_{0.1}Ga_{1.6}S_7$ (*d*) and $Tb_3Fe_{0.1}Ga_{1.6}S_7$ (*e*)

For the $Pr(Nd)_3Fe_{0.1}Ga_{1.6}S_7$ sulfides, the characteristic lines of Pr^{3+} and Nd^{3+} are clearly observed within the band gap and can be assigned to the following transitions from the ground state: 497 nm ($^3P_0$), 608 nm ($^1D_2$), 1020 nm ($^1G_4$), 1385 nm ($^3F_4$), 1405 nm ($^3F_4$) and 1485 nm ($^3F_3$) for Pr^{3+} [33], and to 530 nm ($^2K_{15/2}$, $^2G_{9/2}$, $^2G_{7/2}$), 600 nm ($^2G_{7/2}$, $^4G_{5/2}$), 690 nm ($^4F_9$), 760 nm ($^4S_{3/2}$, $^4F_{7/2}$), 820 nm ($^2H_{9/2}$, $^3F_{5/2}$) and 890 nm ($^4F_{3/2}$) for Nd^{3+} [34].

For the $Ce(Tb)_3Fe_{0.1}Ga_{1.6}S_7$ sulfides, the spectra do not exhibit distinct characteristic lines of Ce^{3+} or Tb^{3+} in the visible or near-infrared regions. This

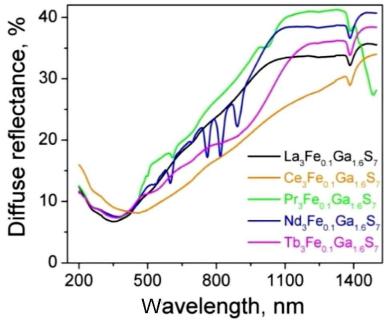

Fig. 4. Diffuse reflectance spectra of $R_3Fe_{0.1}Ga_{1.6}S_7$ (R – La, Ce, Pr, Nd, Tb) sulfide powders at room temperature

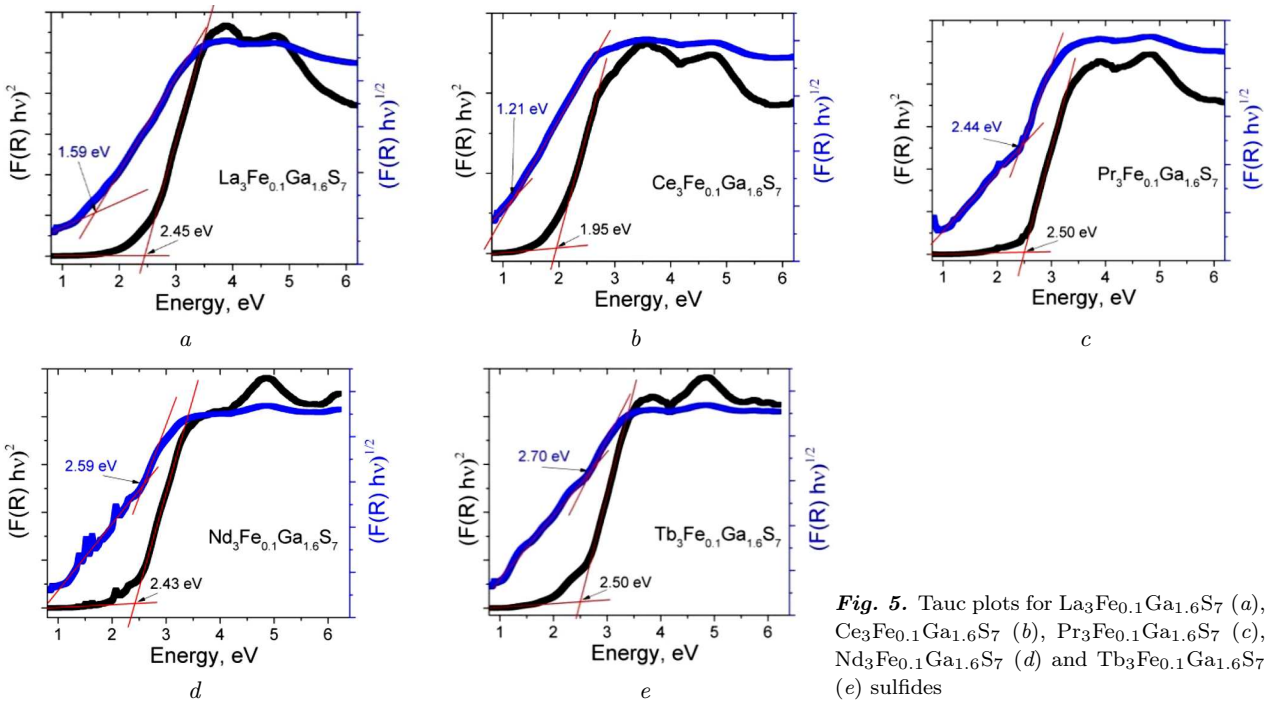

Fig. 5. Tauc plots for $La_3Fe_{0.1}Ga_{1.6}S_7$ (*a*), $Ce_3Fe_{0.1}Ga_{1.6}S_7$ (*b*), $Pr_3Fe_{0.1}Ga_{1.6}S_7$ (*c*), $Nd_3Fe_{0.1}Ga_{1.6}S_7$ (*d*) and $Tb_3Fe_{0.1}Ga_{1.6}S_7$ (*e*) sulfides

is because the electronic states of Ce^{3+} are located in the ultraviolet region ($5d$–$4f$ ($^2F_{7/2}$, $^2F_{5/2}$) transitions at ∼250–350 nm). Meanwhile, the f–f transitions of Tb^{3+} in the visible range, such as transitions from one of the $^7F_{0,1,2,3,4,5,6}$ ground states to the $^5D_4$ excited state at ∼488 nm ($^7F_6$), ∼543 nm ($^7F_5$), ∼584 nm ($^7F_4$), ∼622 nm ($^7F_3$), are inherently weak and further broadened by crystal field effects in the lattice [35, 36].

The band gap energy of the $R_3Fe_{0.1}Ga_{1.6}S_7$ (R – La, Ce, Pr, Nd, Tb) sulfides was determined by extrapolating the linear portion of the Tauc plot to the energy axis for both direct and indirect allowed transitions (Fig. 5).

Analysis of the Tauc plots for the $R_3Fe_{0.1}Ga_{1.6}S_7$ (R = La, Ce, Pr, Nd, Tb) sulfides shows that the representation for direct transitions, $(F(R)h\nu)^2$, exhibits a longer and clearer linear region compared to the indirect case. The obtained results indicate that the investigated phases are characterized by a direct allowed transition with a band gap energy of approximately 1.95–2.50 eV. These values are close to the characteristics of the classical nonlinear optical chalcogenide $AgGaS_2$ (≈2.5–2.7 eV) [37–39], indicating the potential of these compounds for applications in infrared nonlinear optics. The combination of a moderate band gap and the expected high polarizability can provide a favorable balance between the nonlinear optical response and the laser-induced damage threshold. It is also worth noting that among the investigated compounds, the Ce-containing sample stands out due to significantly lower band gap values for both direct and indirect transitions compared to other members of the studied series. No clear correlation was found between the chemical composition and the band gap energy values.

The calculated band structure of the $R_3Fe_{0.1}Ga_{1.6}S_7$ (R – La, Ce) sulfides was plotted along the lines connecting the following high-symmetry points of the first Brillouin zone: Γ → A → → H → K → Γ → M → L → H. The presented band structures are plotted for the energy ranges of –42 to 22 eV (for $La_3Fe_{0.1}Ga_{1.6}S_7$) and –62 to 22 eV (for $Ce_3Fe_{0.1}Ga_{1.6}S_7$). In the energy ranges from 3 to 22 eV (for $La_3Fe_{0.1}Ga_{1.6}S_7$) and from –3 to 22 eV (for $Ce_3Fe_{0.1}Ga_{1.6}S_7$), the band structure is represented by a set of closely spaced bands corresponding to the combined energy levels of the constituent atoms. This part of the electronic spectrum is practically continuous within the specified ranges. For the electronic structure calculations, 0 eV corresponds to the valence band maximum and

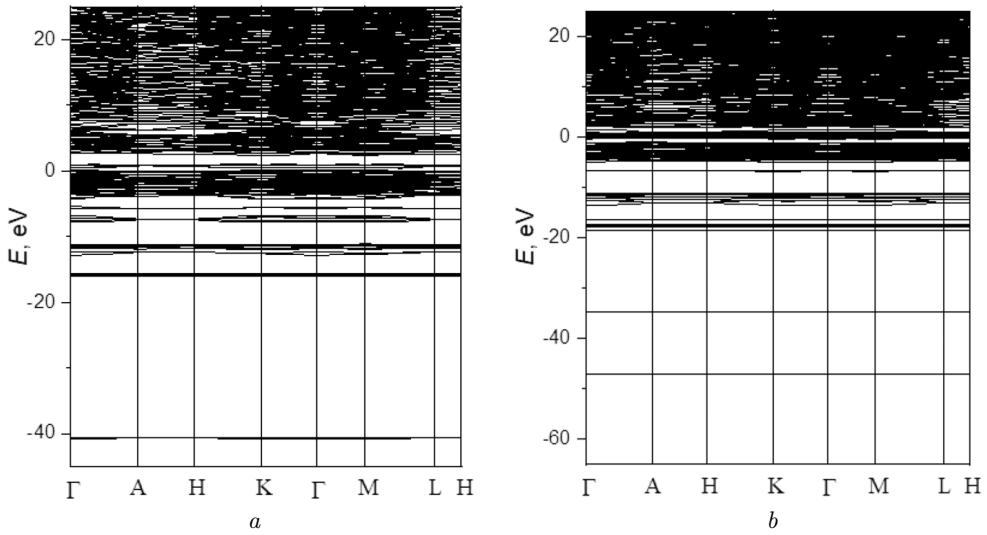

Fig. 6. Band structure of $La_3Fe_{0.1}Ga_{1.6}S_7$ (*a*) and $Ce_3Fe_{0.1}Ga_{1.6}S_7$ (*b*)

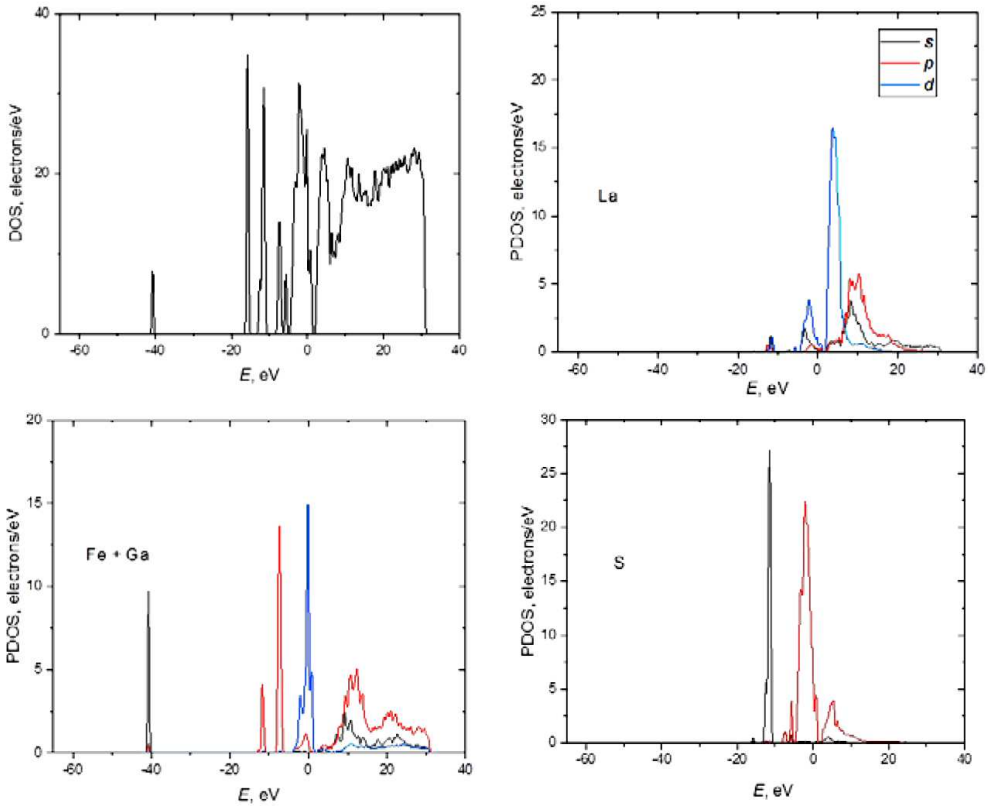

Fig. 7. Total and partial densities of states (DOS/PDOS) of the Fe-substituted lanthanum gallium sulfide $La_3Fe_{0.1}Ga_{1.6}S_7$ calculated using the GGA

coincides with the Fermi energy. Near this energy, a distinct group of energy levels appears, indicating presence of localized states. At lower energies, a set of narrow levels is observed, corresponding to strongly bound core states. The band structure of these sulfides is presented in Fig. 6.

Near 0 eV, which corresponds to the valence band maximum, there is a band formed by the localized

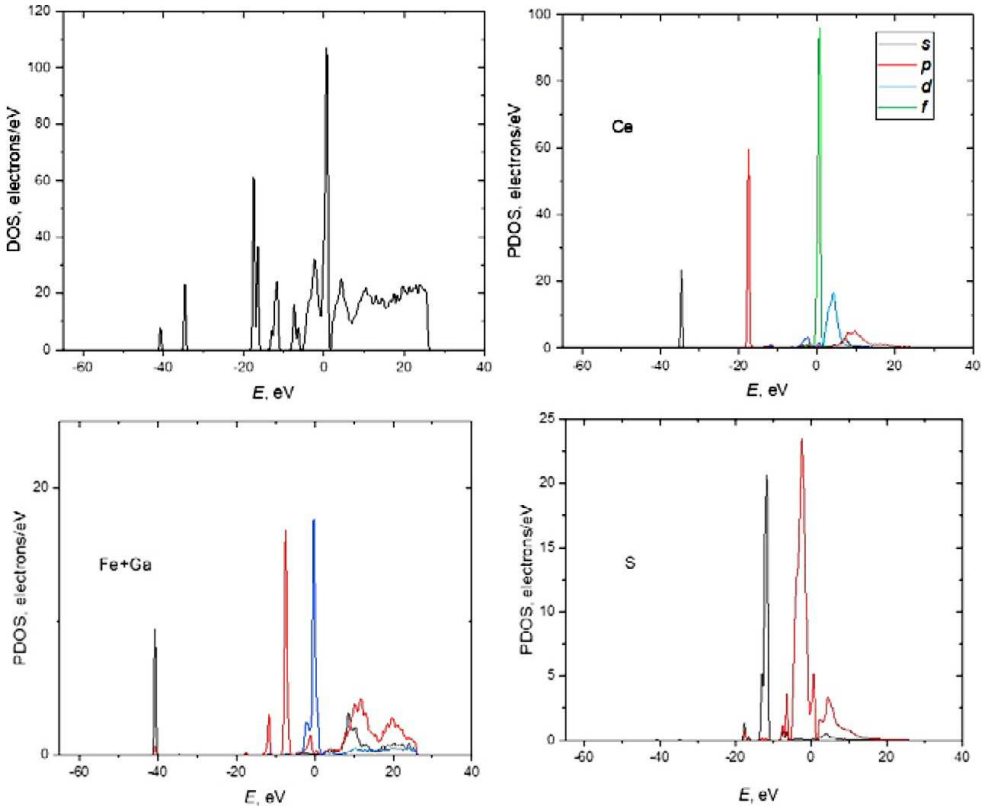

Fig. 8. Total and partial densities of states (DOS/PDOS) Fe-substituted cerium gallium sulfide $Ce_3Fe_{0.1}Ga_{1.6}S_7$ calculated using the GGA

d-states of La, *f*-states of Ce, *d*-states of Fe + Ga and *p*-states of S. The narrow bands near –40 eV, –16 eV, and –13 eV are formed by the *s*- and *p*-states of Fe + Ga. At –12 eV, a high-intensity band with a contribution from the *s*-states of S appears. Within the range of 0 to 20 eV, low-intensity bands of the *p*-states of La and Fe + Ga are observed. In the Ce-containing sulfide, the *s*- and *p*-states of Ce are located at –35 eV and –18 eV, respectively.

The electronic structure of these sulfides differs only in the partial densities of states of the rare-earth elements. Figs 7 and 8 show the total and partial densities of states calculated using the GGA.

The obtained results indicate that the $La(Ce)_3Fe_{0.1}Ga_{1.6}S_7$ sulfides are direct band gap semiconductors with band gap energies in the range of ∼1.95–2.50 eV, which is consistent with the nature of the linear portions of the Tauc plots and indicates efficient optical transitions. Calculations within density functional theory confirm the semiconducting nature of these compounds and demonstrate a complex structure of the valence band, formed predominantly by the *p*-states of S with a noticeable contribution from the *d*-states of metals and, in the case of Ce-containing phases, localized *f*-states. The presence of separated electronic states near the Fermi level may suggest a potential sensitivity of the electronic structure to substitution or external influences.

At the same time, it was established that substituting La for Ce does not alter the overall band structure profile; however, it leads to a redistribution of the partial densities of states. This effect can be utilized as a tool for fine-tuning the electronic and, consequently, optical characteristics. The combination of the experimental and theoretical insights obtained suggests that the investigated sulfides are promising functional materials for optoelectronic applications, where the presence of a direct band gap and a complex electronic structure opens up possibilities for controlling their properties by varying the composition.

4. Conclusions

The crystal structure of $R_3Fe_{0.1}Ga_{1.6}S_7$ (R = La, Ce, Pr, Nd, Tb) sulfides, which crystallize in the hexag-

onal system (space group $P6_3$; La_3CuSiS_7 structural type), was investigated by X-ray powder diffraction.

The hydrodynamic particle sizes of six synthesized sulfide powder samples were measured by the DLS method, and their polydispersity indices were found to lie within the range PDI $\approx$ 0.120–0.155. These values indicate the high stability and homogeneity of the powders, making them suitable for applications in catalysis and nanotechnology.

The band gap energies were determined by optical methods using the Tauc plot method based on the Kubelka - Munk function for the following sulfides: $La_3Fe_{0.1}Ga_{1.6}S_7$ (E_g^* = 1.59 eV; E_g^{**} = 2.45 eV), $Ce_3Fe_{0.1}Ga_{1.6}S_7$ (E_g^* = 1.21 eV; E_g^{**} = 1.95 eV), $Pr_3Fe_{0.1}Ga_{1.6}S_7$ (E_g^* = 2.44 eV; E_g^{**} = 2.50 eV), $Nd_3Fe_{0.1}Ga_{1.6}S_7$ (E_g^* = 2.59 eV; E_g^{**} = 2.43 eV), $Tb_3Fe_{0.1}Ga_{1.6}S_7$ (E_g^* = 2.70 eV; E_g^{**} = 2.50 eV). (E_g^* – direct band gaps; E_g^{**} – indirect band gaps).

The noncentrosymmetric structure of the obtained phases opens up possibilities for their use in nonlinear optical devices. Due to their ability to generate optical harmonics and exhibit self-focusing effects, these sulfides can serve as a basis for the development of new optical converters and functional components for laser systems.

1. O.V. Marchuk, N.M. Blashko, M.Ya. Rudysh, O.A. Yakymchuk. Crystal and band energy structure of $Nd_{1.5}Y(Tb)_{1.5}Ga_{1.67}S_7$ sulfides. *Functional Materials* **33** (1), 15 (2026).
2. N.M. Blashko, O.V. Marchuk, V.M. Kordan. Synthesis and crystal structure of the $R_3Fe_{0.1}Ga_{1.6}Se_7$ selenides (R–La, Ce, Pr, Nd). *Phys. Chem. Solid State* **26** (3), 556 (2025).
3. N.M. Blashko, O.V. Marchuk, A.O. Fedorchuk. The crystal structure of $R_3Fe_{0.1}Ga_{1.6}S_7$ chalcogenides (R–La, Ce, Pr and Tb). *Phys. Chem. Solid State* **25** (4), 677 (2024).
4. N.M. Blashko, O.V. Smitiukh, O.V. Marchuk. The crystal structure of $La_3Pb_{0.1}Ga_{1.6}S_7$ and $Pr_3Pb_{0.1}Ga_{1.6}S_7$ compounds. *Phys. Chem. Solid State* **23** (1), 96 (2022).
5. B.J. Eggleton, B. Luther-Davies, K. Richardson. Chalcogenide photonics. *Nature Photonics* **5** (3), 141 (2011).
6. J.R. Sootsman, D.Y. Chung, M.G. Kanatzidis. New and old concepts in thermoelectric materials. *Angew. Chem. Int. Ed. Engl.* **48**, 8616 (2009).
7. K. Mitchell, J.A. Ibers. Rare-earth transition-metal chalcogenides. *Chem. Rev.* 102 (6), 1929 (2002).
8. M. Ohta, T. Kuzuya, H. Sasaki, T. Kawasaki, S. Hirai. Synthesis of multinary rare-earth sulfides $PrGdS_3$, $NdGdS_3$, and $SmEuGdS_4$, and investigation of their thermoelectric properties. *J. Alloys Comp.* **484**, 268 (2009).
9. M. Wuttig, N. Yamada. Phase-change materials for rewriteable data storage. *Nature Mater.* **6**, 824 (2007).
10. A. K. Iyer, B.W. Rudyk, X. Lin, H. Singh, A.Z. Sharma, C.R. Wiebe, A. Mar, Noncentrosymmetric rare-earth copper gallium chalcogenides $RE_3CuGaCh_7$ (RE = La–Nd; Ch = S, Se): An unexpected combination. *J. Solid State Chem.* **229**, 150 (2015).
11. B.W. Rudyk, S.S. Stoyko, A.O. Oliynyk, A. Mar. Rare-earth transition-metal gallium chalcogenides Re_3MGaCh_7 (M = Fe, Co, Ni; Ch = S, Se). *J. Solid State Chem.* **210** (1), 79 (2014).
12. A.K. Iyer, W. Yin, B.W. Rudyk, X. Lin, T. Nilges, A. Mar. Metal ion displacements in noncentrosymmetric chalcogenides $La_3Ga_{1.67}S_7$, $La_3Ag_{0.6}GaCh_7$ (Ch = S, Se), and La_3MGaSe_7 (M = Zn, Cd). *J. Solid State Chem.* **243**, 221 (2016).
13. He Jianqiao, W. Zhe, Z. Xian, C. Ye, G. Yu, X. Lai, C. Zheng, J. Lin,F. Huang. Synthesis, structure, magnetic and photoelectric properties of $Ln_3M_{0.5}M'Se_7$ (Ln = La, Ce, Sm; M = Fe, Mn; M′ = Si, Ge) and $La_3MnGaSe_7$. *RSC Adv.* **5**, 52629 (2015).
14. Y. Wenlong, S. Youguo, K. Bin, D. Jianguo, Y. Jiyong, Wu Yicheng. Rare-earth transition-metal chalcogenides Ln_3MGaS_7 (Ln = Nd, Sm, Dy, Er; M = Co, Ni) and Ln_3MGaSe_7 (Ln = Nd, Sm, Gd, Dy, M = Co; Ln = Nd, Gd, Dy, M = Ni). *J. Solid State Chem.* **213**, 87 (2014).
15. I. Chung, M.G. Kanatzidis. Metal Chalcogenides: A Rich Source of Nonlinear Optical Materials. *Chem. Mater.* **26**, 849 (2014).
16. A.K. Iyer, W. Yin, E.J. Lee, X. Lin, A. Mar. Quaternary rare-earth sulfides $RE_3M_{0.5}GeS_7$ (RE = La–Nd, Sm; M = Co, Ni) and $Y_3Pd_{0.5}SiS_7$. *J. Solid State Chem.* **250**, 14 (2017).
17. L. Akselrud, Y. Grin. WinCSD: Software package for crystallographic calculations (Version 4). *J. Appl. Cryst.* **47**, 803 (2014).
18. K. Momma, F. Izumi. VESTA 3 for three-dimensional visualization of crystal, volumetric and morphology data. *J. Appl. Cryst.* **44**, 1272 (2011).
19. P. Kubelka, F. Munk. An article on optics of paint layers. *Z. Tech. Phys.* **12**, 593 (1931).
20. J. Tauc, R. Grigorovici, A. Vancu. Optical properties and electronic structure of amorphous germanium. *Phys. Status Solidi* **15**, 627 (1966).
21. W. Kohn, L.J. Sham. Self-consistent equations including exchange and correlation effects. *Phys. Rev.* **140**, 1133 (1965).
22. S. Clark, M. Segall, C. Pickard, P. Hasnip, M. Probert, R. Refson, M. Payne. First principles methods using CASTEP. *Z. Kristallographie – Crystalline Mater.* **220**, 567 (2005).
23. M. Segall, P. Lindan, M. Probert, C. Pickard, S. Hasnip, S. Clark, M. Payne. First-principles simulation: Ideas, illustrations and the CASTEP code. *J. Phys.: Condens. Matter.* **14**, 2717 (2002).
24. L. Bellaiche, D. Vanderbilt. Virtual crystal approximation revisited: Application to dielectric and piezoelectric properties of perovskites. *Phys. Rev. B* **61**, 7877 (2000).

25. D. Hamann, M. Schlüter, C. Chiang. Norm-conserving pseudopotentials. *Phys. Rev. Lett.* **43**, 1494 (1979).
26. J.P. Perdew, K. Burke, M. Ernzerhof. Generalized gradient approximation made simple. *Phys. Rev. Lett.* 77, 3865 (1996).
27. H.J. Monkhorst, J.D. Pack. Special points for Brillonin-zone integrations. *Phys. Rev. B: Solid State.* **13**, 5188 (1976).
28. A.M. Loireau-Lozach, M. Guittard, J. Flahaut. Systemes L_2S_3–Ga_2S_3 (L = La, Ce, Dy, Er et Y). *Mat. Res. Bull.* **12**, 881, (1977).
29. M. Patrie, M. Guittard. Chimie minerale. Sur les composes du type $Ce_6Al_{10/3}S_{14}$. *C. R. Acad. Sci. C* **268**, 1136 (1969).
30. M. Guittard, M. Julien-Pouzol. Les composes hexagonaux de type La_3CuSiS_7. *Bulletin de la Societe Chimique de France* **6**, 2207 (1972).
31. C.G. Ma, M.G. Brik, D.X. Liu, B. Feng, Ya Tian, A. Suchocki. Energy level schemes of f^N electronic configurations for the di-, tri-, and tetravalent lanthanides and actinides in a free state. *J. Lumin.* **170**, 369 (2016).
32. S.W. Yu, M.H. Carpenter, F. Ponce, S. Friedrich, J.S. Lee. Atomic origin of $3d^94f^1$ configuration in La^{3+} solids. *J. Phys.: Condens. Matter.* **27**, 405501 (2015).
33. M. Seshadri, I.T.C. Santos, M.J.V. Bell, J. Lapointe, Y. Messaddeq, V. Anjos. Near-infrared quantum cutting luminescence in Pr^{3+}/Yb^{3+} doped lead bismuth borate glass. *Sci. Rep.* **12**, 19311 (2022).
34. J.A. Jiménez, R. Amesimenu, M. Thomas. Impact of lanthanide (Nd^{3+}, Gd^{3+} and Yb^{3+}) ionic field strength on the structure and thermal expansion of phosphate glasses. *J. Phys. Chem. B* **128** (12), 2995 (2024).
35. M.Y.A. Yagoub, H.C. Swart, E. Coetsee. Energy transfer study between Ce^{3+} and Tb^{3+} ions in a calcium fluoride crystal for solar cell applications. *J. Lumin.* **187**, 96 (2017).
36. S. Kalusniak, T. Castellano-Hernández, H. Yalçinoğlu, H. Tanaka, C. Kränkel. Spectroscopic properties of Tb^{3+} as an ion for visible lasers. *Appl. Phys. B* **128**, 33 (2022).
37. J.-H. Feng, C.-Li Hu, X. Xu, B.-X. Li, M.-J. Zhang, J.-G. Mao. $AgGa_2PS_6$: A new mid-infrared nonlinear optical material with a high laser damage threshold and a large second harmonic generation response. *Chem. – A Europ. J.* **23** (46), 10978 (2017).
38. X. Huang, Q. Wu, R. Dai, J. Ning, L. Zhang, W. Wang, S. Xue, J. Yan, F. Zhang. A density functional study of the structural, electronic, optical and lattice dynamical properties of $AgGaS_2$. *Results in Phys.* **35**, 105309 (2022).
39. T.-J. Wang, H.-Z. Zhang, F.-G. Wu, Z.-S. Feng, H.-Y. Zang, Z.-H. Kang, Y. Jiang, J.-Y. Gao. 3–5 μm $AgGaS_2$ optical parametric oscillator with prism cavity. *Laser Phys.* **19**, 377 (2009).

Received 27.05.26

Н.М. Блашко, О.В. Марчук,
В.М. Греб, Р.Л. Буклів, М.Я. Рудиш

КРИСТАЛОХІМІЯ, ОПТИЧНІ ВЛАСТИВОСТІ ТА ЕЛЕКТРОННА СТРУКТУРА СУЛЬФІДІВ $R_3Fe_{0,1}Ga_{1,6}S_7$ (R – La, Ce, Pr, Nd, Tb)

За результатами рентґенівської порошкової дифрактометрії встановлено кристалохімічні параметри сульфідів складу $R_3Fe_{0,1}Ga_{1,6}S_7$ (R – La, Ce, Pr, Nd, Tb), які кристалізуються у структурному типі La_3CuSiS_7 (просторова група (ПГ) $P6_3$). Кристалічна структура цих сполук сформована взаємопов'язаною тривимірною мережею координаційних поліедрів різного типу, зокрема семикоординованих поліедрів [R S_7], октаедрів змішаного заповнення [M (Fe, Ga) S_6] і тетраедрів [Ga S_4]. Якісний і кількісний елементний склад синтезованих сульфідів підтверджено методами енергодисперсійної рентґенівської спектроскопії в поєднанні із скануальною електронною мікроскопією (EDX/SEM). Розподіл розмірів частинок і ступінь їх однорідності в колоїдних системах (дисперсія в ізопропіловому спирті) охарактеризовано методом динамічного розсіювання світла, на основі чого визначено індекси полідисперсності. Оптичні параметри сульфідів встановлено із застосуванням методу Тауца: ширина забороненої зони становить від 1,95 до 2,50 еВ для прямих міжзонних переходів і від 1,21 до 2,70 еВ для непрямих, що свідчить про варіативність електронної структури залежно від складу. Для сульфідів, що містять La і Ce, проведено квантово-хімічне моделювання в рамках теорії функціонала густини (DFT, *ab initio* підхід), у межах якого розраховано зонну структуру.

Ключові слова: рідкісноземельні елементи, енергодисперсійний рентґенівський аналіз, порошкова рентґенівська дифрактометрія, метод графіків Тауца, метод функціонала густини.